A New Image Reconstruction Strategy for Capacitively Coupled Electrical Impedance Tomography

Yimin Wu[1], Yandan Jiang[1*], Haifeng Ji[1], Baoliang Wang[1], Zhiyao Huang[1] and Manuchehr Soleimani[2]

[1] Department One, State Key Laboratory of Industrial Control Technology, College of Control Science and Engineering, Zhejiang University, Hangzhou 310027, China
[2] Department Two, Engineering Tomography Laboratory (ETL), Department of Electronic and Electrical Engineering, University of Bath, Bath BA2 7AY, UK

E-mail: ydjiang@zju.edu.cn

Received xxxxxx
Accepted for publication xxxxxx
Published xxxxxx

Abstract

Capacitively coupled electrical impedance tomography (CCEIT) is an attractive improvement of electrical resistance tomography (ERT) that offers contactless measurement and utilizes both the real and imaginary parts of the impedance for monitoring conductive gas-liquid two-phase flows in the industry. The conventional CCEIT adopts finite element method (FEM) under the benchmark of conductive liquid background to obtain the sensitivity matrices, which has been validated effective in ERT for the usage of the real part information. However, few researches on the usage of the imaginary part information of the conductive fluid have been reported. More research work should be undertaken to seek the most effective sensitivity calculation benchmark for the imaginary part utilization in CCEIT. In this work, the usage of the imaginary part information under different sensitivity calculation benchmarks is studied and a new image reconstruction strategy is proposed accordingly for CCEIT. By comparing the imaginary part sensitivity matrices and the corresponding imaging performance under different backgrounds, the benchmark that can make better use of the imaginary part information is determined. With the determined benchmark, a new image reconstruction strategy of CCEIT, which utilizes the respective effective benchmarks for the image reconstruction of the two parts of the fluid impedance, respectively, and employs a novel hybrid image fusion method to obtain the final image, is presented. Research results show that the benchmark of non-conductive gas background is more effective for the usage of the imaginary part information of the conductive gas-liquid two-phase flow. Experimental results demonstrate the effectiveness of the proposed strategy in obtaining high-quality images. Compared with the conventional image reconstruction strategy of CCEIT, the proposed strategy has better imaging performance. This research provides valuable experience in utilizing the imaginary part information of the fluid impedance and lays a good foundation for the further development of CCEIT.

Keywords: electrical resistance tomography (ERT), capacitively coupled electrical impedance tomography (CCEIT), sensitivity matrix, image reconstruction, image fusion

1. Introduction

Electrical resistance tomography (ERT) is known as an important kind of electrical tomography (ET) technique [1]-[7]. With the advantages of simple structure, no radiation, high speed and low cost, it has shown great potential in the state monitoring and parameter measurement of conductive gas-liquid two-phase flows in industrial processes [7]-[9]. However, the traditional ERT still has some limitations: 1) It requires contact measurement, which causes polarization, electrochemical erosion and contamination of the electrodes in practical applications [9]-[11]. 2) It uses the real part or the amplitude of the impedance, which leads to insufficient usage of the impedance information, especially the imaginary part information [12]-[16].

To avoid the above problems, capacitively coupled electrical impedance tomography (CCEIT) was proposed as an improvement of ERT. By referring to the idea of the capacitively coupled contactless conductivity detection (C^4D) technique, CCEIT implements contactless measurement of the fluid impedance [17]. That means the problems resulting from contact measurement in the traditional ERT no longer exist in CCEIT. Meanwhile, inspired by the research results that both the real part and imaginary part of the fluid impedance contain useful information [17]-[22], CCEIT regards the gas-liquid two-phase flow as a complete impedance and uses both the two parts for imaging. Therefore, CCEIT has attracted much attention from researchers since it was proposed and has shown great potential in industrial applications [8]-[10], [20]-[22].

In the past several years, significant progress has been achieved in CCEIT [15], [20]-[22]. It has been verified that utilizing both the real and imaginary parts of the fluid impedance makes sense in improving the imaging performance [23]-[26]. But as a new technique, CCEIT is still developing and needs further investigation. Image reconstruction is to solve the inverse problem and obtain the phase distribution image via image reconstruction algorithms. The process relies on a pre-calculated sensitivity matrix and a projection vector derived from the impedance measurements. The sensitivity matrix allows for the transformation of the acquired measurements into the representation of the internal phase distribution [27]-[29]. So, in addition to the image reconstruction algorithm, the sensitivity matrix is also a crucial factor to ensure the accuracy of the image reconstruction results. However, previous CCEIT-related researches mainly focus on seeking effective image reconstruction algorithms. There is a lack of targeted research on the sensitivity matrix calculation of CCEIT.

The finite element method (FEM) is a widely applied method to obtain the sensitivity matrix in the field of ERT, where a conductivity change is introduced to each element/pixel under a reference background (benchmark) for sensitivity calculation [30]. ERT takes the conductive liquid phase of the gas-liquid two-phase flow as the benchmark. As the improvement of ERT, CCEIT also followed the FEM under the conductive background in ERT for sensitivity calculation. That means both the real part sensitivity matrix and imaginary part sensitivity matrix in the conventional CCEIT technique are calculated under the benchmark of conductive liquid background. Although studies on ERT have validated that the sensitivity calculation under the conductive background is more suitable for the utilization of the real part information, few researches on the usage of the imaginary part information of the conductive fluid have been undertaken. Our experience and knowledge of the sensitivity calculation of the imaginary part under different benchmarks are very limited. Therefore, research and attempt should be conducted to seek the most effective sensitivity calculation benchmark for the imaginary part of the conductive fluid, and implement more effective usage of the fluid impedance by CCEIT.

In this work, the usage of the imaginary part information of the conductive gas-liquid two-phase flow under different benchmarks is investigated. To seek the most sensitivity calculation benchmark for the imaginary part, imaginary part sensitivity matrices under the benchmarks of conductive liquid background and non-conductive gas background are both calculated. The corresponding sensitivity characteristics and imaging performance of the imaginary part under the two backgrounds are compared. Further, a new image reconstruction strategy for CCEIT is proposed, where the image reconstruction of the real and imaginary parts is implemented under the respective sensitivity calculation benchmarks, and a hybrid image fusion method is proposed to further improve the image quality of CCEIT. Finally, experiments will be carried out to verify the effectiveness of the proposed image reconstruction strategy.

The innovative ideas of this work are:

1) Targeted research on the utilization of the imaginary part information of the conductive gas-liquid two-phase flow in CCEIT is addressed. By seeking an effective sensitivity calculation benchmark, better utilization of the imaginary part information of the fluid impedance is realized and better image reconstruction results of the imaginary part are obtained.

2) A new image reconstruction strategy is proposed for CCEIT to take full advantage of the impedance information. On the one hand, the real part and imaginary part sensitivity matrices are calculated respectively under the most effective benchmark of each, and the reconstruction of high-quality real part image and imaginary part image is implemented, respectively. On the other hand, a hybrid image fusion method is proposed to further exploit and fuse the information in the two reconstructed images, and obtain the higher-quality final image.

The remainder of this paper is organized as follows. Section 2 shows the principle of CCEIT. Section 3 elaborates on the investigation and comparison of the imaginary part sensitivity matrix, including sensitivity matrices under different benchmarks and reconstruction of the imaginary part images. Section 4 shows the proposed image reconstruction strategy. The experimental setup and results are presented in Section 5. The conclusions are drawn in Section 6.

2. Principle of CCEIT

Figure 1 shows the measurement principle of CCEIT [23]-[25]. As shown in figure 1(a), in a 12-electrode CCEIT sensor, 12 identical metal electrodes are uniformly distributed over the outside surface of the insulating pipe, avoiding direct contact with the fluid.

CCEIT takes the 1-electrode excitation and 1-electrode detection strategy, i.e., for each impedance measurement, one electrode is selected as the excitation electrode and one electrode is selected as the detection electrode, and other electrodes are kept floating [21]. In a measurement cycle, a frame of data has 66 independent impedance measurements, including 66 real part measurements and 66 imaginary part measurements. As shown in figure 1, labeling the 12 electrodes as e1, e2, …, e12 and taking the electrode pair e4-e10 as an example, the equivalent circuit of a measurement electrode pair can be represented by two coupling capacitances C_4, C_{10} and in series with an impedance $Z_{4,10}$. C_4 and C_{10} are formed by the electrode e4 and e10 with the insulating pipe and the conductive fluid inside the pipe, respectively. $Z_{4,10}$ is the equivalent impedance of the fluid between the two electrodes (e4 and e10). When an AC voltage source is applied to e4, an output current can be obtained at e10 for the impedance measurement. The equivalent impedance measured by the electrode pair can be described as [20]-[22]:

$$Z_{4,10} = R + jX \tag{1}$$

where R is the real part of the impedance and X is the imaginary part of the impedance.

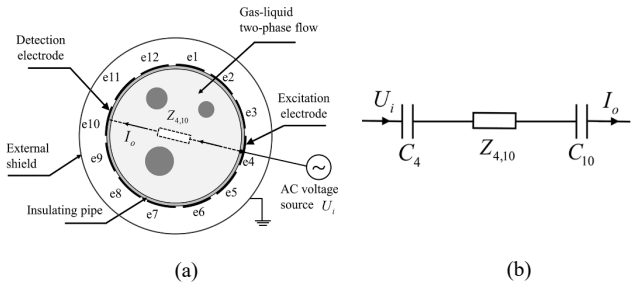

Figure 1. (a) Cross-section schematic diagram of the 12-electrode CCEIT sensor. (b) Equivalent circuit of a measurement electrode pair (e4-e10).

3. On the Imaginary Part Sensitivity Matrix

In this section, an investigation on the influence of the sensitivity calculation benchmark on the utilization of the imaginary part information in CCEIT is carried out. The imaginary part sensitivity matrices under two different benchmarks, the conductive liquid background and the non-conductive gas background, are calculated and compared to seek the most effective benchmark for the imaginary part.

3.1 Modelling of CCEIT under different benchmarks

The sensing field of the CCEIT sensor can be regarded as a quasi-static electromagnetic field. According to Maxwell's equations, the relationship between the distribution of electrical properties (resistance property and capacitance property) and the potential distribution in the CCEIT sensing field Ω satisfies the following mathematical model:

$$\nabla[\gamma(x,y)\nabla\varphi(x,y)] = 0, (x,y) \in \Omega \tag{2}$$

where $\gamma(x,y) = \sigma(x,y) + j\omega\varepsilon(x,y)$ is the complex conductivity distribution of the medium in Ω. $\sigma(x,y)$, $\varepsilon(x,y)$ and $\varphi(x,y)$ are the conductivity, permittivity and potential at the spatial point of coordinates (x,y) within Ω, respectively. According to the excitation-detection strategy of the CCEIT system, the boundary conditions of (2) are as follows:

$$\begin{cases} \varphi(x,y) = U_i, (x,y) \in \Gamma_e \\ \varphi(x,y) = 0, (x,y) \in \Gamma_d \\ \partial\varphi(x,y)/\vec{n} = 0, (x,y) \in \Gamma_f \end{cases} \tag{3}$$

where Γ_e, Γ_d and Γ_f represent the spatial regions of the excitation electrode, the detection electrode and the floating electrodes, respectively. $\vec{n}$ denotes the outward unit normal vector.

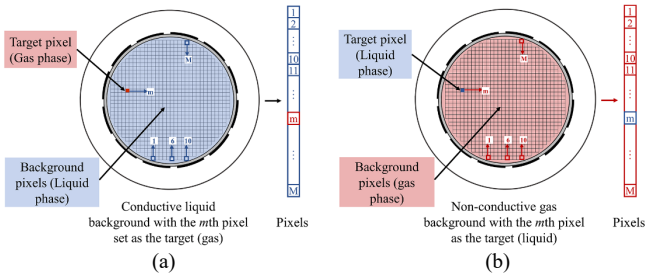

Figure 2. Geometric model and field domain setting of CCEIT under different benchmarks. (a) The conductive liquid background; (b) The non-conductive gas background.

As mentioned, the FEM-based sensitivity calculation by simulation depends on a reference background (benchmark). In conventional CCEIT, the conductive liquid background of the gas-liquid two-phase flow is taken as the benchmark in the sensitivity calculation of either the real part or the imaginary part. Figure 2(a) shows the geometric model and field domain setting of CCEIT under the conventional benchmark, where the background pixels are filled with the conductive liquid phase and the non-conductive gas phase is introduced to the target pixel one by one for sensitivity calculation [20]. This conductive benchmark is widely accepted in the traditional ERT and has been validated effective for the utilization of the real part information. However, few researches on the usage of the imaginary part information of the conductive fluid have been undertaken. To seek a suitable benchmark for the imaginary part of CCEIT, further research on the sensitivity calculation of the imaginary part under different benchmarks is needed. Therefore, the non-conductive benchmark is also investigated for the utilization of the imaginary part. Figure 2(b) shows the geometric model and field domain setting of CCEIT under the non-conductive gas background (benchmark), where the background pixels are set as the gas phase and the target pixel is set as the liquid phase for sensitivity calculation.

With the electromagnetic models in (2) and (3), and the geometric models and field domain settings in figure 2, the imaginary part sensitivity matrices under different benchmarks can be calculated. Specifically, for any electrode pair, an AC voltage source U_i is applied to the excitation electrode, and the impedance of the two models can be calculated from the complex currents I_o^L and I_o^G, which are collected on the detection electrode, respectively. The

complex currents I_o^L and I_o^G under the two backgrounds can be computed from the integration of the current densities J_o^L and J_o^G in the region of the detection electrode, respectively:

$$I_o^L = \int_{\Gamma_d} J_o^L d\Gamma_d \tag{4}$$

$$I_o^G = \int_{\Gamma_d} J_o^G d\Gamma_d \tag{5}$$

Therefore, the imaginary part X^L under the conductive liquid background and the imaginary part X^G under the non-conductive gas background are obtained as:

$$X^L = \mathrm{Im}\,(U_i / I_o^L) \tag{6}$$

$$X^G = \mathrm{Im}\,(U_i / I_o^G) \tag{7}$$

where Im denotes taking the imaginary part.

Then, the imaginary part sensitivity matrix under the conductive liquid background $S^{XL} = \left[s_{nm}^{XL}\right]_{N\times M}$ and the imaginary part sensitivity matrix under the non-conductive gas background $S^{XG} = \left[s_{nm}^{XG}\right]_{N\times M}$ can be calculated as:

$$s_{nm}^{XL} = \left(X_{nm}^L - X_{n0}^L\right) \Big/ X_{n0}^L,\ m = 1,2...,M,\ n = 1,2,...N \tag{8}$$

$$s_{nm}^{XG} = \left(X_{nm}^G - X_{n0}^G\right) \Big/ \left(X_{n0}^L - X_{n0}^G\right),\ m = 1,2...,M,\ n = 1,2,...N \tag{9}$$

where s_{nm}^{XL} and s_{nm}^{XG} are the sensitivities between the *n*th imaginary part measurement and the *m*th pixel under the conductive liquid background and the non-conductive gas background, respectively. X_{n0}^L denotes the *n*th imaginary part measurement when all the pixels are set as the liquid phase and X_{n0}^G denotes the *n*th imaginary part measurement when all the pixels are set as the gas phase, respectively. X_{nm}^L denotes the *n*th imaginary part measurement when the *m*th pixel changes from the liquid phase to the gas phase and the rest pixels keep unchanged as the liquid phase, as shown in figure 2(a). X_{nm}^G denotes the *n*th imaginary part measurement when the *m*th pixel changes from the gas phase to the liquid phase and the rest pixels keep unchanged as the gas phase, as shown in figure 2(b). N is the number of independent impedance measurements, and M is the number of the pixels in FEM. In this work, $N = 66$ and $M = 820$. Here, the liquid phase is set with the conductivity of $\sigma_1 = 0.002$ S/m and the relative permittivity of $\varepsilon_1 = 78$, and the gas phase is set with the conductivity of $\sigma_2 = 0$ S/m, and the relative permittivity of $\varepsilon_2 = 1$.

Figure 3 shows six typical sensitivity distributions of the two imaginary part sensitivity matrices obtained by the six typical measurement electrode pairs e1-e2, e1-e3, …, e1-e7. The sensitivity distributions in figure 3(a) are obtained under the conductive liquid background and those in figure 3(b) are obtained under the non-conductive liquid background. To quantitatively evaluate the sensitivity distributions, the average sensitivity s_a and the uniformity coefficient s_u are introduced, and the calculations are as follows [21]:

$$s_a = \sum_{n=1}^{6}\sum_{m=1}^{M} s_{nm} \Big/ l \tag{10}$$

$$s_u = \sum_{n=1}^{6} v_n \Big/ 6 s_a^n \tag{11}$$

where l is the total number of positive sensitivities in the six distributions. v_n and s_a^n are the standard deviation and the average sensitivity of the sensitivities in the *n*th sensitivity distribution, respectively.

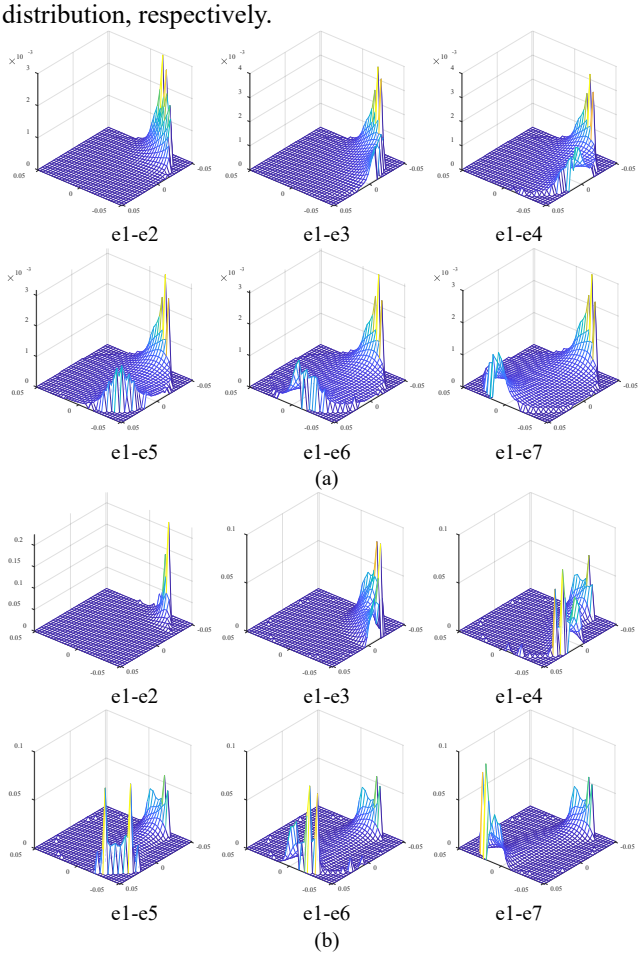

Figure 3. Six typical sensitivity distributions under the two benchmarks. (a) Conductive liquid background. (b) Non-conductive gas background.

Table 1. Indexes of the typical sensitivity distributions.

Benchmark	Evaluation indexes	
	s_a	s_u
Conductive liquid background	0.00019	1.647
Non-conductive gas background	0.00292	3.301

Generally, the average sensitivity describes the average response of the sensor to small changes in the sensing area, and the uniformity coefficient means the differences of the sensitivities in the sensitivity field [21]. Thus, higher average sensitivity and lower uniformity coefficient are preferred. Table I shows the two indexes of the typical sensitivity distributions of the imaginary part under the two benchmarks. It is found that although the conductive liquid background contributes to obtaining a more uniform sensitivity distribution, the non-conductive gas background helps improve the average sensitivity of the imaginary part to the target by an order of magnitude. To make a comprehensive comparison, the imaging performance of the imaginary part with the two imaginary part sensitivity matrices should also be investigated.

3.2 Imaging performance of the two sensitivity matrices

Image reconstruction of the imaginary part is implemented with the imaginary part sensitivity matrices calculated under the two benchmarks, respectively. The image reconstruction can be expressed as:

$$P = S\Lambda \tag{12}$$

where $P=[p_1,p_2,\dots p_n,...,p_N]^T$ is the projection vector. $S=[s_{nm}]_{N\times M}$ is the sensitivity matrix. $\Lambda=[\lambda_1,\lambda_2,\dots,\lambda_m,...,\lambda_M]$ is the gray value vector of the reconstructed image.

According to (8) and (9), the imaginary part projection vectors under the two benchmarks P_{XL} and P_{XG} can be calculated from the impedance measurements as:

$$p_{XL,n}=\left(X_n-X_{n0}^L\right)\Big/X_{n0}^L \tag{13}$$

$$p_{XG,n}=\left(X_n-X_{n0}^G\right)\Big/\left(X_{n0}^L-X_{n0}^G\right) \tag{14}$$

where X_n represents the nth imaginary part measurement when the sensing field is filled with the unknown distribution to be reconstructed. $p_{XL,n}$ and $p_{XG,n}$ denote the nth projections in the two imaginary part projection vectors, respectively.

To make a comparison of the imaging performance of the two imaginary part sensitivity matrices, several image reconstruction algorithms such as linear back projection (LBP), simultaneous iterative reconstruction technique (SIRT) algorithm, conjugate gradient (CG) algorithm and Landweber iteration algorithm, are adopted for image reconstruction [31], [32]. LBP algorithm is known as a classic image reconstruction algorithm, which has the advantage of simplicity and is a widely used algorithm to obtain the initial image for other algorithms. Therefore, in this work, the initial inputs for all the iterative algorithms are obtained by LBP algorithm.

Table 2. Imaginary part images of CCEIT reconstructed with sensitivity matrices calculated under the two benchmarks.

Water conductivity			0.002S/m				0.0002S/m			
Experimental setup	True distribution	Benchmark	LBP	SIRT	CG	Landweber	LBP	SIRT	CG	Landweber
S1		Conductive liquid background								
		Non-conductive gas background								
S2		Conductive liquid background								
		Non-conductive gas background								
S3		Conductive liquid background								
		Non-conductive gas background								

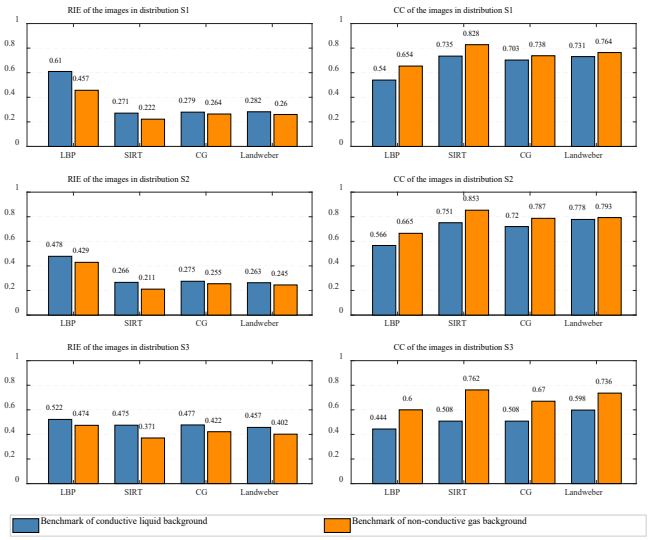

Figure 4. Quantitative evaluation of the imaginary part images reconstructed with sensitivity matrices calculated under the two benchmarks with the water conductivity of 0.002S/m.

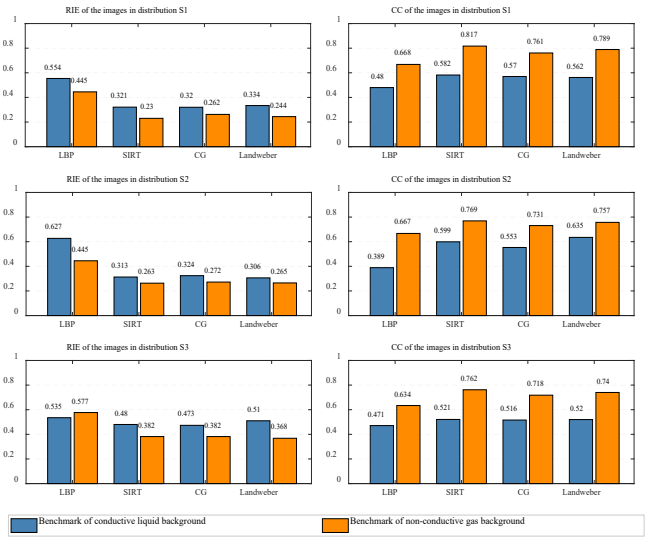

Figure 5. Quantitative evaluation of the imaginary part images reconstructed with sensitivity matrices calculated under the two benchmarks with the water conductivity of 0.02S/m.

Two evaluation criteria, namely, the relative image error (RIE) and the correlation coefficient (CC), are introduced to quantitatively evaluate the reconstructed images. The corresponding formulas are as follows:

$$\mathrm{RIE} = \sqrt{\sum_{m=1}^{M}(\lambda_m - \hat{\lambda}_m)^2} \Big/ \sqrt{\sum_{m=1}^{M}\hat{\lambda}_m^2} \quad (15)$$

$$\mathrm{CC} = \sum_{m=1}^{M}(\lambda_m - \bar{\lambda})(\hat{\lambda}_m - \bar{\hat{\lambda}}) \Big/ \sqrt{\sum_{m=1}^{M}(\lambda_m - \bar{\lambda})^2 \sum_{m=1}^{M}(\hat{\lambda}_m - \bar{\hat{\lambda}})} \quad (16)$$

where $\hat{\lambda}_m$ and λ_m are, respectively, the true and reconstructed gray value of the *m*th pixel, $\bar{\hat{\lambda}}$ and $\bar{\lambda}$ are the mean values of the true and reconstructed gray value vector,.

Experiments were carried out with a 12-electrode CCEIT system to obtain the imaginary part measurements. Three experimental setups S1–S3 were tested, where water with the conductivities of 0.002 S/m and 0.02 S/m were used to simulate the conductive liquid phase, and non-conductive plastic rods with diameters of 30mm and 40mm were used to simulate the non-conductive gas phase, respectively. Table 2 shows the imaginary part images reconstructed under the two benchmarks. Figure 4 and 5 show the corresponding quantitative evaluation.

As shown in table 2, the imaginary part images under both of the two benchmarks can reflect the actual distribution in most cases, especially the positions of the plastic rods. It is indicated that the imaginary part of the impedance of the conductive gas-liquid two-phase flow contains useful information of the phase distribution. And utilizing the imaginary part of the fluid impedance for image reconstruction is effective. According to the quantitative evaluation in figure 4 and figure 5, comparing the reconstructed images under the two benchmarks, the imaging performance of the imaginary part under the non-conductive gas background outperforms that under the conductive liquid background. It is found that adopting the non-conductive benchmark for the conductive fluid can reconstruct higher-quality imaginary part images. This advantage is consistent across various image reconstruction algorithms and becomes more pronounced for the gas-liquid two-phase flow with higher conductivity liquid phase. That means the benchmark of the non-conductive background of the conductive fluid enables more effective utilization of the imaginary part information.

4. The new Image Reconstruction Strategy

Based on the research results obtained in Section 3, a new image reconstruction strategy, which can make better use of the impedance information, is proposed for CCEIT. In this strategy, real part and imaginary part images are reconstructed under the respective effective benchmarks, and a hybrid image fusion method is proposed to integrate the two images.

Figure 6 shows the overview of the proposed image reconstruction strategy. First, impedance measurements (the real part and the imaginary part) of the gas-liquid two-phase flow are obtained by a 12-electrode CCEIT system. Then, image reconstruction is implemented by using the LBP+SIRT algorithm to reconstruct the real and imaginary part images, respectively, where "LBP + SIRT" denotes that the initial image/input of the SIRT algorithm is obtained by the LBP algorithm. The real part image is reconstructed with the real part of the impedance measurements and the real part sensitivity matrix calculated under the conventional benchmark of conductive liquid background. The imaginary part image is reconstructed with the imaginary part of the impedance measurements and the imaginary part sensitivity matrix under the benchmark of non-conductive gas background. Finally, a hybrid image fusion method, which introduces arithmetic average fusion, subtractive fusion and logical filtering algorithm, is proposed to fuse the two images and obtain the final image.

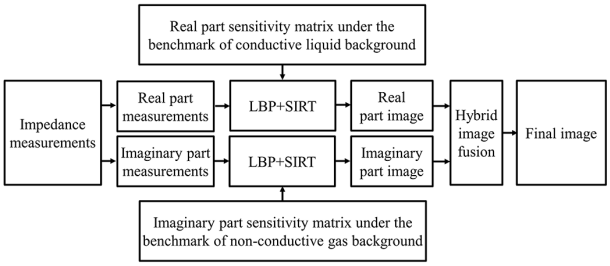

Figure 6. Overview of the new image reconstruction strategy.

4.1 Image reconstruction of the two parts

The real part image $\Lambda^{RL} = [\lambda_m^{RL}]_{M\times 1}$ can be obtained under the conventional benchmark of the conductive liquid background by the SIRT iterative algorithm:

$$\lambda_m^{RL(i)} = \lambda_m^{RL(i-1)} + \frac{1}{N}\sum_{n=1}^{N} s_{nm}^{RL}\left(\frac{p_{RL,n} - \sum_{m=1}^{M} s_{nm}^{RL}\lambda_m^{RL(i-1)}}{\sum_{m=1}^{M}(s_{nm}^{RL})^2}\right) \quad (17)$$

where $\lambda_m^{RL(i)}$ and $\lambda_m^{RL(i-1)}$ are the *m*th gray value of the real part image in the *i*th and *i*-1th iterations, respectively. $p_{RL,n}$ is the *n*th projection in the real part projection vector, which is calculated by $p_{RL,n} = \left(R_n^L - R_{n0}^L\right)/R_{n0}^L$. R_{n0}^L represents the *n*th real part measurement when the pipe is filled with the liquid background. R_n^L represents the *n*th real part measurement when the pipe is filled with the unknown distribution to be reconstructed. s_{nm}^{RL} is the real part sensitivity between the *n*th real part measurement and the *m*th pixel under the conductive liquid background. Similar to (6), Re which denotes taking the real part can be applied to obtain the real part as $R^L = \mathrm{Re}\,(U_i / I_o^L)$. Then, the calculation of s_{nm}^{RL} in the real part sensitivity matrix $S^{RL} = [s_{nm}^{RL}]_{N\times M}$ is similar to the calculation of that in the imaginary part sensitivity matrix under the conductive liquid background shown in (8). More details of the real part sensitivity matrix can also be found in [20], [21]. The initial value of the gray value vector for SIRT, i.e., the initial image $\lambda_m^{RL(0)}$, is reconstructed by LBP:

$$\lambda_m^{RL(0)} = \sum_{n=1}^{N} s_{nm}^{RL} p_{RL,n} \Big/ \sum_{n=1}^{N} s_{nm}^{RL} \tag{18}$$

Similarly, the imaginary part image $\Lambda^{XG} = [\lambda_m^{XG}]_{M\times 1}$ under the benchmark of non-conductive gas background can be obtained as:

$$\lambda_m^{XG(i)} = \lambda_m^{XG(i-1)} + \frac{1}{N}\sum_{n=1}^{N} s_{nm}^{XG}\left(\frac{p_{XG,n} - \sum_{m=1}^{M} s_{nm}^{XG}\lambda_m^{XG(i-1)}}{\sum_{m=1}^{M}(s_{nm}^{XG})^2}\right) \tag{19}$$

where $\lambda_m^{XG(i)}$ and $\lambda_m^{XG(i-1)}$ are the mth gray value of the real part image in the ith and i-1th iterations, respectively. And the initial image $\lambda_m^{XG(0)}$ is also reconstructed by LBP:

$$\lambda_m^{XG(0)} = \sum_{n=1}^{N} s_{nm}^{XG} p_{XG,n} \Big/ \sum_{n=1}^{N} s_{nm}^{XG} \tag{20}$$

4.2 The hybrid image fusion method

To integrate the impedance information in the two images and obtain higher-quality final image, a new hybrid image fusion method is developed by taking advantage of arithmetic average fusion, subtractive fusion and logical filtering algorithm.

The arithmetic average fusion is a classic pixel-level fusion method with high computational efficiency [33]. However, it suffers from the disadvantages of blurred image edges and the inability to eliminate image artifacts [33], [34]. Therefore, the image quality is not satisfactory and improvement is usually required. The subtractive fusion algorithm also plays an important role in conventional image fusion [34], [35]. It mines the difference information between the images, which is not available to the arithmetic average fusion algorithm. From this aspect, combining the average information and the difference information of the real and imaginary part images might be a good idea to obtain better-fused results. But it is important to seek an effective algorithm to make the trade-off between the average information and the difference information. That can be done by the logical filtering algorithm, which is good at integrating different information through logical operations [21], [35]. With this algorithm, a higher-quality reconstructed image is expected by exploiting and integrating the real image, the imaginary image, and the average and difference information of them. Based on these considerations, the proposed hybrid image fusion method includes the following three steps:

1) Obtain the average image of the real and imaginary part images by arithmetic average fusion:

$$\lambda_m^{ave} = (\lambda_m^{RL} + \lambda_m^{XG})/2 \tag{21}$$

where λ_m^{ave} denotes the gray value of the mth pixel in the average image.

2) Obtain the difference image of the real and imaginary part images by subtractive fusion:

$$\lambda_m^{diff} = \left|\lambda_m^{RL} - \lambda_m^{XG}\right| \tag{22}$$

where λ_m^{diff} is the gray value of the mth pixel in the difference image and $|\cdot|$ denotes taking the absolute value.

3) Obtain the final reconstructed image by logical filtering algorithm. This step is designed according to the following findings: a) When the mth pixels in the two images are both calculated to be the gas phase, the mth pixel tends to be the gas phase. b) When the mth pixels in the two images are both calculated to be the liquid phase, it is more probable to be the liquid phase. c) When the difference of the gray values of the mth pixels in the two images is large, the mth pixel is more likely to be a noise point or the artifact, making the arithmetic average fusion ineffective. To reduce the influence of this pixel, the difference information of the two images should be removed properly from the average image. So, this step can be described as:

$$\lambda_m^{final} = \begin{cases} 1, \text{ if } \lambda_m^{RL} > \tau_h \text{ and } \lambda_m^{XG} > \tau_h \\ 0, \text{ if } \lambda_m^{RL} < \tau_l \text{ and } \lambda_m^{XG} < \tau_l \\ \max(0, \lambda_m^{ave} - \lambda_m^{diff}), \text{ others} \end{cases} \tag{23}$$

where λ_m^{final} denotes the gray value of the mth pixel in the final image, τ_h and τ_l are the high and low thresholds of the logic filter, which are determined by:

$$\begin{aligned} \tau_h &= \sum_{m=1}^{M} \lambda_m^{ave} \Big/ \text{count}_h,\ st.\lambda_m \geq \overline{\lambda}^{ave} \\ \tau_l &= \sum_{m=1}^{M} \lambda_m^{ave} \Big/ \text{count}_l,\ st.\lambda_m < \overline{\lambda}^{ave} \end{aligned} \tag{24}$$

where $\overline{\lambda}^{ave}$ is the mean gray value of the pixels in the average image. count_h and count_l are the total numbers of pixels whose gray values are above and below the mean gray value of the pixels in the average image, respectively. So, in the logic filter in (23), τ_h serves as an indicator for determining whether the mth pixel belongs to the gas phase and τ_l is taken as the indicator for determining whether the mth pixel belongs to the liquid phase.

5. Results

To verify the effectiveness of the proposed image reconstruction strategy, image reconstruction experiments were carried out with the 12-electrode CCEIT system. Figure 7(a) shows the structure of the 12-electrode CCEIT system for experiments. It consists of three parts, namely the 12-electrode CCEIT sensor, the signal processing unit and the industrial personal computer (IPC). Figure 7(b) shows the photo of the 12-electrode CCEIT system. In the experiments, water with the electrical properties of $\sigma_1(x,y) = 0.002$ S/m and $\varepsilon_1(x,y) = 78$ was used to simulate the liquid phase. Plastic rods with different diameters or air with the electrical properties of $\sigma_2(x,y) = 0$ S/m and $\varepsilon_2(x,y) = 1$ were used to simulate the gas phase. Five distributions S4-S8 were tested, as shown in figure 8.

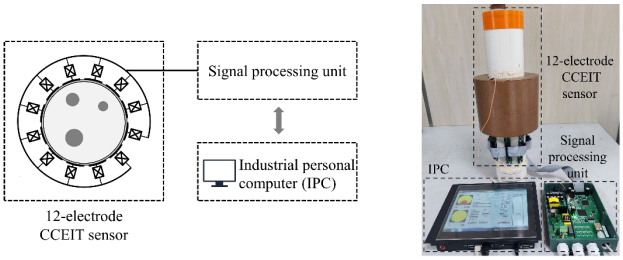

Figure 7. The 12-electrode CCEIT system. (a) Structure. (b) Photo.

Figure 8 shows the ground truth distributions and the imaging results. In figure 8, the top two rows of images ("experimental setup" and "true distribution") display the ground truth distributions. The row marked as "real part" exhibits the real part images obtained with the real part sensitivity matrix under the benchmark of conductive liquid background. The row of "imaginary part under the conductive benchmark" shows the imaginary part images obtained with the imaginary part sensitivity matrix under the benchmark of conductive liquid background. The row of "imaginary part under the non-conductive benchmark" shows the imaginary part images obtained with the imaginary part sensitivity matrix under the benchmark of non-conductive gas background. The row labeled "conventional CCEIT" shows the reconstructed images using the conventional image reconstruction strategy of CCEIT, where the classical arithmetical average fusion algorithm is applied to fuse the real part image and imaginary image under the conductive benchmark. The row of "conventional CCEIT with the hybrid image fusion method" presents the reconstructed images, where the conventional image reconstruction strategy is still used but the proposed hybrid image fusion method is applied to fuse the real part image and imaginary image under the conductive benchmark. Finally, the row marked as "the proposed strategy for CCEIT" illustrates the reconstructed images obtained by the proposed image reconstruction strategy for CCEIT. All the real part images and imaginary part images are reconstructed by SIRT. The corresponding evaluation criteria of RIE and CC are shown below the images.

It could be drawn from figure 8:

1) The presented image reconstruction strategy for CCEIT is effective. The images obtained by the new strategy are in good accordance with the actual distributions. Compared with the images obtained by the conventional CCEIT where the real part and imaginary part sensitivity matrices are calculated under the same benchmark, the final images obtained by the proposed strategy have higher image quality. That means using respective optimized benchmarks for the real part sensitivity calculation and imaginary part sensitivity calculation in CCEIT is an effective way to implement better utilization of the impedance information.

2) Introducing the non-conductive gas background as the benchmark to take full advantage of the imaginary part of the impedance is valid. The information usage of the imaginary part is more effective under the non-conductive benchmark. Compared with the imaginary images obtained under the conductive benchmark, higher-quality imaginary images are reconstructed under the non-conductive benchmark.

3) The proposed hybrid image fusion method is successful in optimizing the usage of the impedance information. It can effectively exploit the differences and similarities between the real part and imaginary part images to further improve the image quality. Compared with the classical arithmetical average fusion algorithm, the proposed hybrid image fusion method can obtain better-fused images.

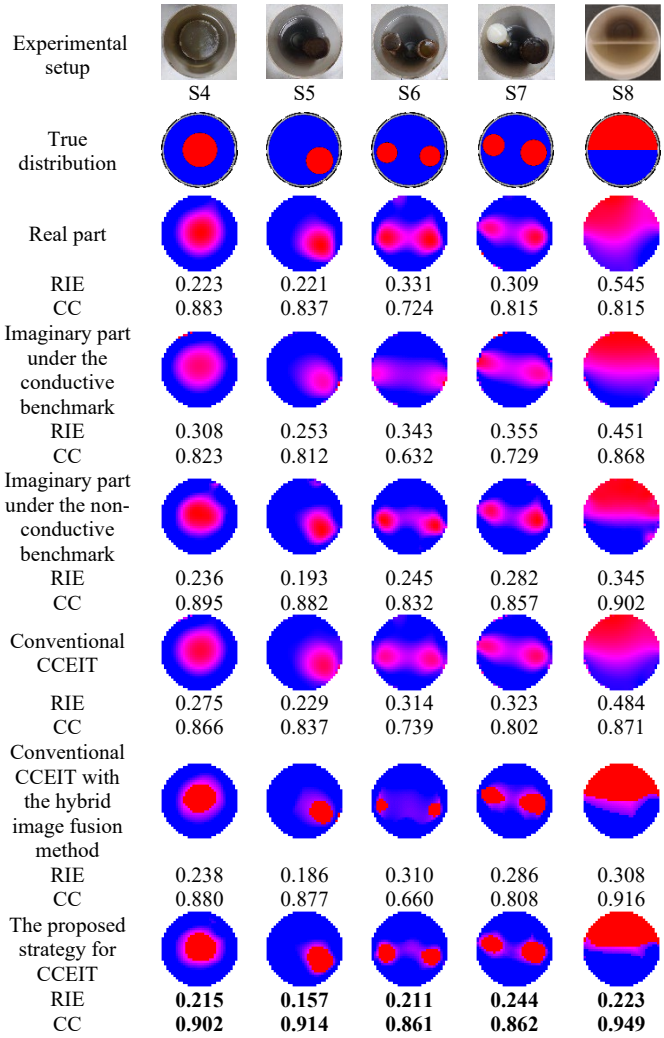

Figure 8. The reconstructed images under LBP + SIRT algorithm (S4: one plastic rod with the diameter of 50mm in water; S5: one plastic rod with the diameter of 39 mm in water; S6: two plastic rods with diameters of 30mm and 30mm in water; S7: two plastic rods with diameters of 32mm and 39mm in water; S8: stratified flow with air as the gas phase and water as the liquid phase).

Besides, to investigate the generalization performance of the proposed new image reconstruction strategy (the real part under conductive benchmark + the imaginary part under non-conductive benchmark + the hybrid image fusion method), investigation was conducted under other image reconstruction algorithms, including the LBP + CG algorithm and the LBP +

Landweber algorithm. The experimental setup S4~S8 is the same as that in figure 8. Figure 9 and figure 10 depict the reconstructed images by using the LBP + CG algorithm and the LBP + Landweber algorithm, respectively. The corresponding evaluation criteria of RIE and CC are presented below the images. It is indicated that compared with the conventional CCEIT method, the proposed strategy has consistently superior performance under different image reconstruction algorithms, highlighting its good generalization ability.

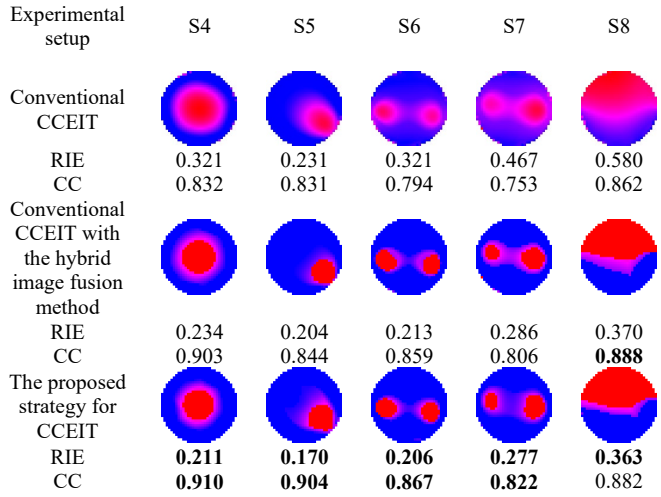

Figure 9. The reconstructed images under LBP + CG algorithm.

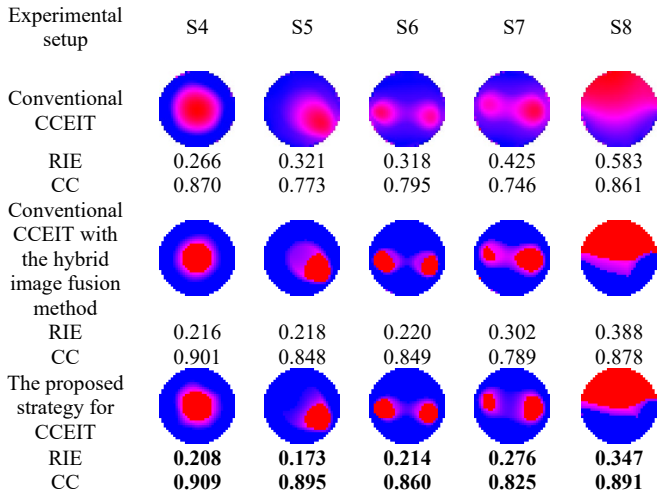

Figure 10. The reconstructed images under LBP + Landweber algorithm.

The above experimental results further verified that employing respective optimized benchmarks for the real part and imaginary part sensitivity calculation in CCEIT can realize more effective utilization of the impedance information, and the new hybrid image fusion method is effective in integrating the two parts of the impedance.

Notably, the high threshold τ_h and low threshold τ_l are critical parameters for the hybrid image fusion method. In this work, the threshold values of τ_h and τ_l are determined automatically by (23) and (24), according to the gray values of the pixels in the average image. However, it is important to investigate the influence of these two parameters on the image reconstruction strategy. Therefore, the fused images obtained by (23) with four different threshold combinations of τ_h and τ_l are investigated for comparison, i.e., Threshold combination A ($\tau_h = 0.9$ and $\tau_l = 0.1$), Threshold combination B ($\tau_h = 0.8$ and $\tau_l = 0.2$), Threshold combination C ($\tau_h = 0.7$ and $\tau_l = 0.3$), Threshold combination D ($\tau_h = 0.6$ and $\tau_l = 0.4$). Figure 11 shows the comparison results, where all the setup is the same as that of the proposed strategy in figure 8 except for the values of the two thresholds. It is found that the values of the two thresholds do have influence on the quality of the fused image. So, it is critical to determine reasonable threshold values. Compared with the Threshold combination A~D, the thresholds automatically determined by (24) in the proposed hybrid image fusion method have the overall best performance and exhibit a more consistent performance across different distributions. That means determining the threshold values of τ_h and τ_l by (24) here is reasonable and effective.

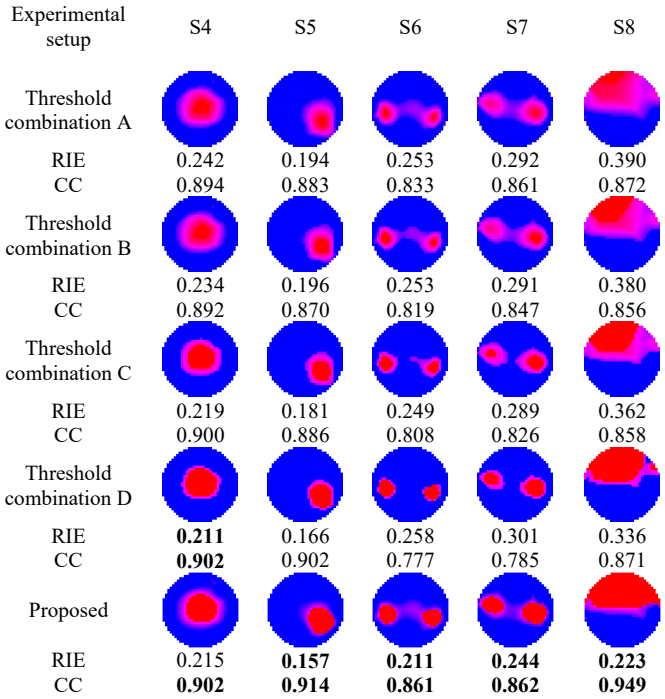

Figure 11. The fused images obtained by (23) with different threshold combinations of τ_h and τ_l.

Furthermore, considering that the speed of image reconstruction plays an important role in real-time

applications, we conducted a comparative analysis on the reconstruction time of different methods under LBP + SIRT algorithm. The results are shown in table 4. It is found that compared with the conventional CCEIT using the classical arithmetical average fusion algorithm, slightly increased reconstruction time can be observed in the conventional CCEIT with the hybrid image fusion method, which can be attributed to the additional time required for the threshold calculation in (24). Compared with the conventional CCEIT method, the proposed strategy also exhibits a slightly longer reconstruction time but is in the same order of magnitude. With the LBP + SIRT algorithm adopted as for real and imaginary part image reconstruction, the maximum reconstruction time for the test distributions is 73.14 ms.

Table 4. Reconstruction time of different methods under LBP + SIRT algorithm.
Time-unit (Milli-second)

Method	Experimental setup				
	S4	S5	S6	S7	S8
Conventional CCEIT	5.73	6.33	71.69	27.88	43.77
Conventional CCEIT with the hybrid image fusion method	5.84	6.44	71.85	28.00	43.89
The proposed strategy for CCEIT	9.87	8.97	73.14	30.99	41.29

Notation: The operation system of the test environment is Windows 11, the CPU is AMD Ryzen 7 5800H with Radeon Graphics @3.20 GHz, the memory of the computer is 16.00 GB, programming software is MATLAB 2021a.

6. Conclusions

This work investigates the usage of the imaginary part information of conductive gas-liquid two-phase flows in CCEIT and proposes a new image reconstruction strategy. To seek the most effective benchmark for the sensitivity calculation of the imaginary part, the imaginary part sensitivity matrices under both the conductive background and the non-conductive background are studied. By comparing the sensitivity characteristics and the imaging performance of the two matrices, it is found that the benchmark of non-conductive gas background is more effective in the utilization of the imaginary part information. Based on this, a new image reconstruction strategy is proposed for CCEIT. First, image reconstruction is conducted by LBP + SIRT for the two parts of the impedance under the respective benchmarks, respectively. The real part image is reconstructed with the real part sensitivity matrix under the benchmark of conductive liquid background, and the imaginary part image is reconstructed with the sensitivity matrix under the benchmark of non-conductive gas background. Then, a novel hybrid image fusion method, which combines arithmetic average fusion, subtractive fusion and logical filtering algorithm, is proposed to integrate the real part and imaginary part images and obtain a higher-quality final image.

Experimental results verify the effectiveness and potential of the proposed image reconstruction strategy. By taking full advantage of the real part and imaginary part information under the most effective benchmark of each, high-quality real part and imaginary part images can be obtained. Besides, the proposed hybrid image fusion method can effectively exploit the information in the real and imaginary images to further improve the image quality of CCEIT. Compared with the conventional image reconstruction strategy of CCEIT, the proposed strategy has better imaging performance. The maximum RIE and minimum CC of the final images are 0.244 and 0.861, respectively. Besides, it is indicated that compared with the conventional CCEIT method, the proposed strategy also has consistently superior performance under other algorithms (LBP + CG algorithm and LBP + Landweber algorithm), highlighting its good generalization ability across different image reconstruction algorithms.

Few researches on using the imaginary part information of the conductive gas-liquid two-phase flow have been reported in the conventional ERT. The research in this work provides new knowledge and experience of the influence of sensitivity calculation benchmark on the usage of the imaginary part information. In addition, the proposed image reconstruction strategy can make full use of the real and imaginary parts of the fluid impedance, which lays a good foundation for the follow-up research of CCEIT and provides an effective way to obtain high-quality images. The hybrid image fusion method achieves more effective image fusion by integrating the difference and similarity information between the images, which also provides a useful reference for others' researches.

Acknowledgments

This work was supported in part by the National Natural Science Foundation of China under Grant 62201502, in part by the Natural Science Foundation of Zhejiang Province under Grant LQ22F030001 and in part by the State Key Laboratory of Industrial Control Technology (Zhejiang University) under Grant ICT2023A09.

References

[1] A Adler, D Holder 2021 *Electrical impedance tomography: methods, history and applications* (Florida, United States: CRC Press)

[2] M Wang 2015 *Industrial Tomography: systems and applications* (Amsterdam, Netherlands: Elsevier)

[3] Ø Isaksen 1996 A review of reconstruction techniques for capacitance tomography *Meas. Sci. Technol.* **7** 325–37
[4] Z Cui, Q Wang, Q Xue, W Fan, L Zhang, Z Cao, B Sun, H Wang and W Yang 2016 A review on image reconstruction algorithms for electrical capacitance/resistance tomography *Sens. Rev* **36** 429–45
[5] W Q Yang and L Peng 2003 Image reconstruction algorithms for electrical capacitance tomography *Meas. Sci. Technol.* **14** R1–13
[6] S Liu, Y Huang, H Wu, C Tan and J Jia 2021 Efficient Multitask Structure-Aware Sparse Bayesian Learning for Frequency-Difference Electrical Impedance Tomography *IEEE Trans. Ind. Inf.* **17** 463–72
[7] G Liang, S Ren and F Dong 2021 Coplanar electrical/ultrasonic dual-modality tomography for water continuous gas/oil/water three-phase distribution imaging *Meas. Sci. Technol.* **32** 124004
[8] Y A Wahab, R A Rahim, M H F Rahiman, S R Aw, F R M Yunus, C L Goh, H Abdul Rahim and L P Ling 2015 Non-invasive process tomography in chemical mixtures – A review *Sens. Actuators B Chem.* **210** 602–17
[9] D Xu, X Li and S Zhang 2022 A CCERT-Based Tactile Sensor With Bidirectional Buffer *IEEE Sens. J.* **22** 19480–9
[10] Y A Wahab, R A Rahim, L Pei Ling, M H F Rahiman, S R Aw, F R M Yunus and H Abdul Rahim 2018 Optimisation of electrode dimensions of ERT for non-invasive measurement applied for static liquid–gas regime identification *Sens. Actuators A Phys.* **270** 50–64
[11] S Han, G Yu, W Lu, B Xue, X Gao and Y Song 2023 Fast artifact filtering algorithm for electrical resistivity tomography *Meas. Sci. Technol.* **34** 065601
[12] H Ji, Y Chang, Z Huang, B Wang and H Li 2016 A new contactless impedance sensor for void fraction measurement of gas–liquid two-phase flow *Meas. Sci. Technol.* **27** 124001
[13] C L Yang, A Mohammed, Y Mohamadou, T I Oh and M Soleimani 2015 Complex conductivity reconstruction in multiple frequency electrical impedance tomography for fabric-based pressure sensor *Sensor Review* **35** 85–97
[14] M Zhang and M Soleimani 2016 Simultaneous reconstruction of permittivity and conductivity using multi-frequency admittance measurement in electrical capacitance tomography *Meas. Sci. Technol.* **27** 025405
[15] Q Wang, X Jia and M Wang 2020 Fuzzy Logic Based Multi-Dimensional Image Fusion for Gas–Oil-Water Flows With Dual-Modality Electrical Tomography *IEEE Trans. Instrum. Meas.* **69** 1948–61
[16] X Gao, Z Cao, Y Tian, L Xu and W Yang 2020 Inverse Radon Method Based on Electrical Field Lines for Dual-Modality Electrical Tomography *IEEE Trans. Instrum. Meas.* **69** 8250–60
[17] B Wang, Y Hu, H Ji, Z Huang and H Li 2012 A novel electrical resistance tomography system based on C4D technique *IEEE Trans. Instrum. Meas.* 62 1017–1024
[18] R K Rasel, Q Marashdeh and F L Teixeira 2018 Toward Electrical Capacitance Tomography of Water-Dominated Multiphase Vertical Flows *IEEE Sens. J.* **18** 10041
[19] L Zhu, L Ma, Y Li, Y Yang and M Zhang 2021 Linearization Point and Frequency Selection for Complex-Valued Electrical Capacitance Tomography *IEEE Trans. Instrum. Meas.* **70** 4505011
[20] X Wang, W Xi, B Wang, B Dang and H Hu 2023 An Image Construction Based on the VTLF Fusion Technique for Oil–Water Two-Phase Flow of Noncontact Electrical Impedance Tomography *IEEE Trans. Instrum. Meas.* **72** 9501214
[21] Y Jiang, J Huang, H Ji, B Wang, Z Huang and M Soleimani 2022 Study on Dual-Frequency Imaging of Capacitively Coupled Electrical Impedance Tomography: Frequency Optimization *IEEE Trans. Instrum. Meas.* **71** 4505718
[22] Y Jiang, X He, B Wang, Z Huang and M Soleimani 2020 On the Performance of a Capacitively Coupled Electrical Impedance Tomography Sensor with Different Configurations *Sens.* **20** 5787
[23] H Ji, W Tan, Z Gui, B Wang, Z Huang, H Li and G Wu 2016 A New Dual-Modality ECT/ERT Technique Based on C^4D Principle *IEEE Trans. Instrum. Meas.* **65** 1042–50
[24] H Wu, C Tan and F Dong 2016 An on-line adaptive estimation method for water holdup measurement in oil–water two-phase flow with a conductance/capacitance sensor *Meas. Sci. Technol.* **27** 074001
[25] J Sun and W Yang 2015 A dual-modality electrical tomography sensor for measurement of gas–oil–water stratified flows *Meas.* **66** 150–60
[26] Y Wang, H Ji, Z Huang, B Wang and H Li 2019 Study on image reconstruction of capacitively coupled electrical impedance tomography (CCEIT) *Meas. Sci. Technol.* **30** 094002
[27] M Ding, S Yue, J Li, Y Wang and H Wang 2019 Second-order sensitivity coefficient based electrical tomography imaging *Chem. Eng. Sci.* **199** 40–9
[28] Y Yang, J Liu and G Liu 2023 Image reconstruction for ECT based on high-order approximate sensitivity matrix *Meas. Sci. Technol.* **34** 095402
[29] R C Youngquist, J M Storey, M A Nurge and C J Biagi 2023 A derivation of the electrical capacitance tomography sensitivity matrix *Meas. Sci. Technol.* **34** 025404
[30] A Seppänen, L Heikkinen, T Savolainen, A Voutilainen, E Somersalo and J P Kaipio 2007 An experimental evaluation of state estimation with fluid dynamical models in process tomography *Che. Eng. J.* **127** 23–30
[31] C L Yang, A Mohammed, Y Mohamadou, T I Oh and M Soleimani 2015 Complex conductivity reconstruction in multiple frequency electrical impedance tomography for fabric-based pressure sensor *Sens. Rev.* **35** 85–97
[32] D Chen, B Goris, F Bleichrodt, H H Mezerji, S Bals, K J Batenburg, G De With and H Friedrich 2014 The properties of SIRT, TVM, and DART for 3D imaging of tubular domains in nanocomposite thin-films and sections *Ultramicroscopy* **147** 137–48
[33] S Li, X Kang, L Fang, J Hu and H Yin 2017 Pixel-level image fusion: A survey of the state of the art *Inf. Fusion* **33** 100–12
[34] H B Mitchell 2010 Image Fusion: *Theories, Techniques and Applications* (Berlin, Germany: Springer)
[35] S Ashraf, L Brabyn, and B J Hicks 2012 Image data fusion for the remote sensing of freshwater environments *Appl. Geogr.* **32** 619-628